POLITECNICO
MILANO 1863

Course of Space Propulsion
School of Industrial Engineering

ERMES

CubeSat: design of a bipropellant system

953004	Donato	Giuseppe
939985	Faillace	Antonio
945677	Foligno	Paola Pia
945648	Fontan	Anna
944656	Giambelli	Federico
870132	Gravina	Davide
953335	Gusmaroli	Pietro
946174	Lorenzini	Federico
946172	Mancuso	Antongiacomo
946441	Mori	Paolo

AY 2019-2020

Contents

List of Figures

List of Tables

We thanks professors Filippo Maggi
and Stefano Dossi for their
availability and professionalism.

Nomenclature

Dimensional quantities:

A	Area	$[m^2]$
P_b	Burst pressure	[Pa]
D	Diameter	[m]
L^*	Characteristic length	[m]
c_G	Centre of gravity	[m]
M	Mass	[kg]
P	Pressure	[Pa]
α	Angle of the divergent part of the nozzle	[deg]
β	Angle of the convergent part of the nozzle	[deg]
I_{sp}	Gravimetric specific impulse	[s]
θ_i	Inflection angle of the nozzle	[deg]
θ_e	Exit angle of the nozzle	[deg]
$I_{sp,V}$	Volumetric specific impulse	$[\frac{kg}{m^3 \cdot s}]$
I_{TOT}	Total specific impulse	$[N \cdot s]$
T	Temperature	[K]
F	Thrust	[N]
μ	Dynamic viscosity	$[Pa \cdot s]$
r	Radius	[m]
t	Thickness	[m]
ρ	Density	$[\frac{kg}{m^3}]$
M_m	Molar mass	$[\frac{kg}{kmol}]$
c_P	Specific heat at constant pressure	$[\frac{KJ}{kg \cdot mol}]$
c_V	Specific heat at constant volume	$[\frac{KJ}{kg \cdot mol}]$
t_b	Burning time	[s]
v	Velocity	$[\frac{m}{s}]$
V	Volume	$[m^3]$

Constants:

R	Universal gas constant	$8314 \frac{J}{kmol \cdot K}$
g_0	Gravitational constant	$9.807 \frac{m}{s^2}$

Non dimensional quantities:

ϵ	Area ratio
k	Specific heat ratio
k_l	Minor losses coefficient
λ_l	Non-laminar head losses coefficient
n_m	Mass ratio
OF	Oxidizer to fuel ratio
N	Number of injectors orifices
λ	Divergence loss factor

SYMBOLS:

CC	Combustion chamber
C_d	Discharge coefficient
U	Unity of CubeSat
in	Initial
fin	Final
p	Propellant
Rao	Rao nozzle
OX	Oxidizer
h	Hole
PL	Payload
F	Fuel
e	Exit
t	Throat
conv	Convergent
div	Divergent

ABSTRACT

During the last decade space has become more accessible also thanks to the development of the CubeSats, that are formed by modular and standardized platforms (UNIT). With this new technology a small payload can be used to fulfil low cost space mission. The current limit of this technology is the absence of dedicated propulsion, overcoming this limit will lead CubeSats to be a protagonist in space exploration. For this purpose, in this report the design of a propulsion system for a payload formed by a single UNIT is described. The carried out study has produced as a result an overall 6 UNITs CubeSat, having as propulsion system a bi-propellant liquid engine. In the design process the choice of the propellant couple is followed by the sizing and the positioning of the micro-propulsion technologies (thrust chamber, injector plate, nozzle, tanks), later the performances are computed, the inert masses and the centre of gravity, finally an analysis of the possible failure mode is performed.

P_{CC}	0.7 MPa
ϵ	75
r_{CC}	0.01 m
Δv	600 $\frac{m}{s}$

Table 1: Fixed quantities.

Number of unit	6
Maximum mass	1.33 kg
Volume	1 dm^3
Structural mass	0.1 kg

Table 2: Fixed values for a unit.

T_{CC}	3031.60 K
M_m	20.379 $\frac{kg}{kmol}$
c_P	2156.1 $\frac{J}{K kg}$

Table 3: Values from CEA.

	$\rho[\frac{kg}{m^3}]$	$\mu[\mathbf{Pa \cdot s}]$
NTO:	1447	0.413
MMH:	870.2	0.876

Table 4: Characteristics of the propellants (NTO, MMH).

	Alloy	$\rho[\frac{kg}{m^3}]$	F_{TU}**[MPa]**
Tanks [8]:	Ti-6Al-4V	4420	1000
Tubes [12]:	Ti-3Al-2.5V	4480	620
Nozzle and CC [2]:	INCONEL 718	8190	1100

Table 5: Characteristics of the materials related to the tanks (MMH, NTO, $N_{2(g)}$), tubes and nozzle.

1 Motivation and literature survey

Nowadays, CubeSats are released into space as a secondary payload, in proximity of a primary spacecraft. Propulsion systems often place restrictions on handling, storage, and operations that may limit a CubeSat's ability to launch as a secondary payload. Additionally, being launched in a quasi-nominal orbit means lower accuracy in the location of the CubeSat; nowadays a new challenge is to design a primary propulsion unit that enables higher Δv and larger accelerations, then robust primary propulsion systems become indispensable for interplanetary missions [15].

The reasons why CubeSats need a primary propulsion can be summarised as followed:

- drag compensation and orbit maintenance;
- orbital manoeuvring, including Hohmann transfer;
- synchronization and positioning of communication equipment and payload instruments;
- de-orbiting at the end of the mission to prevent the obstruction of the lower orbit;
- constellation deployment and formation flights.

The primary mission of the CubeSat Program is to provide access to space for small payloads. The propulsion systems can be classified into two types: electric (resistojet, electrospray, ion, Hall and pulsed plasma) and non-electric (cold gas, liquid and solid rocket) systems [5].

The analysed system occupies 6 units. As the manual of the design specifications [17] states, this configuration has been largely employed throughout several missions [11]. Indeed, the 6U provides standardized development for larger picosatellites.

2 Concept description

The assigned task is to design a CubeSat with a bi-propellant primary propulsion system, capable of a long term in-space propulsion and of providing a Δv_{TOT} of $600\frac{m}{s}$ with a maximum acceleration of 3g.
The CubeSat needs to carry a scientific payload of 1U which is 10x10x10 cm. The starting point lies on the decision of the number of the subcomponents of the CubeSat itself. For this purpose: 1U has been assigned to the payload, 1U for the CC and the nozzle, 1U for each propellant tank and 2U for the pressurizing gas.
Hence the CubeSat is composed by a total amount of 6U, a design described in the CubeSat Program [17] with its own specifications (see Fig. 1). Thus the following configuration is stated: the payload at the centre, with the combustion chamber and the nozzle directly below, and the tanks on its sides.

2.1 Additional constraints

As it is evident, the main constraint is related to the CubeSat geometry, therefore the focus should be put on the length of the motor, as the CC, the nozzle and the payload must not exceed 226 mm in the axial direction.
For this reason the room left for the thrust chamber, the injection plate and feeding lines must not overcome 126 mm.

2.2 Propellant selection (CEA)

The selection of the propellant is one of the most important decision. Since the following mission is a long-term one in the outer space, one should be prone in selecting a storable couple. In addition, one should select the propellant in order to transport the lowest possible amount of dry mass. Furthermore, one should select the couple providing the highest possible I_{sp}. This parameter, besides being the most remarkable performance value, is the one responsible for minimizing the overall mass (see Tab. 19). The choice has fallen upon MMH (Mono-Methyl-Hydrazine) and

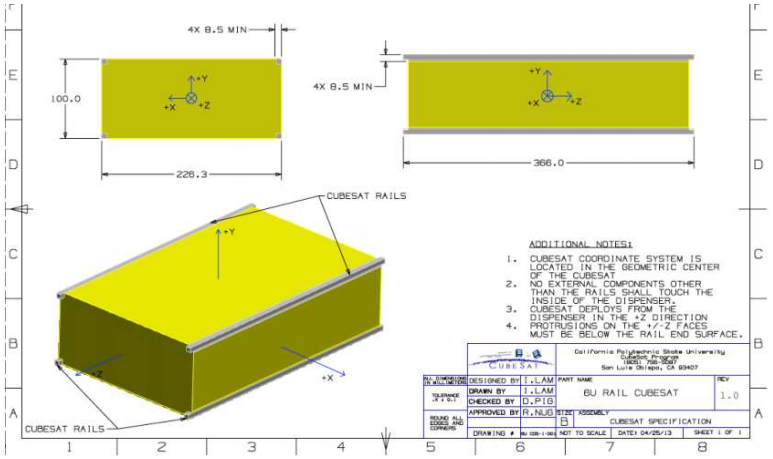

Figure 1: Configuration of the CubeSat

Propellant combination	Combustion chamber characteristic length (L^*), in.
Chlorine trifluoride/hydrazine-base fuel	30-35
Liquid fluorine/hydrazine	24-28
Liquid fluorine/liquid hydrogen (GH_2 injection)	22-26
Liquid fluorine/liquid hydrogen (LH_2 injection)	25-30
Hydrogen peroxide/RP-1 (including catalyst bed)	60-70
Nitric acid/hydrazine-base fuel	30-35
Nitrogen tetroxide/hydrazine-base fuel	30-35
Liquid oxygen/ammonia	30-40
Liquid oxygen/liquid hydrogen (GH_2 injection)	22-28
Liquid oxygen/liquid hydrogen (LH_2 injection)	30-40
Liquid oxygen/RP-1	40-50

Figure 2: L* length

NTO (Nitrous Tetroxide) since they are both storable, hypergolic (no need of an ignition device, saving mass, simpler and also more reliable) and with a low L* (parameter stating the reactive capability of the mixture and related to the final L_{CC} [13]) (see Fig. 2).
For the CEA computation and for motor sizing a P_{CC} of 0.7 MPa is imposed due to multiple reasons. Firstly, the propulsion unit is used for such a small application and so a pressure-fed system is preferable; secondly the engine works in space, so there is no point in elevating the pressure in the CC due to the fact that a complete expansion will never be possible.
After some iterations, the OF is selected as 1.65. This value is the one that maximises the effective velocity in frozen expansion ($U_{eff} = I_{sp}g_0$) (see Fig. 3). The CEA analysis for the combustion is performed with a rocket problem and an expansion with frozen composition at the combustor. This procedure has been decided in order to have the most conservative value on the performances for a preliminary design phase. For the expansion, the ratio is set to 75 (the reasons are going to be explained in the following section).

2.3 Engine design

After the selection of the propellant couple, the definition of the mission and the geometrical constraints, the engine sizing is carried out.
Firstly, the selection of the ϵ has been performed as previously mentioned (see section 2.2). Since this engine is for in-space applications, this parameter should be in a range between 70 and 150. For the following task, a 75 expansion ratio is chosen [1]. This choice is a compromise between performances of the motor and geometrical constraints provided by the CubeSat dimensions.

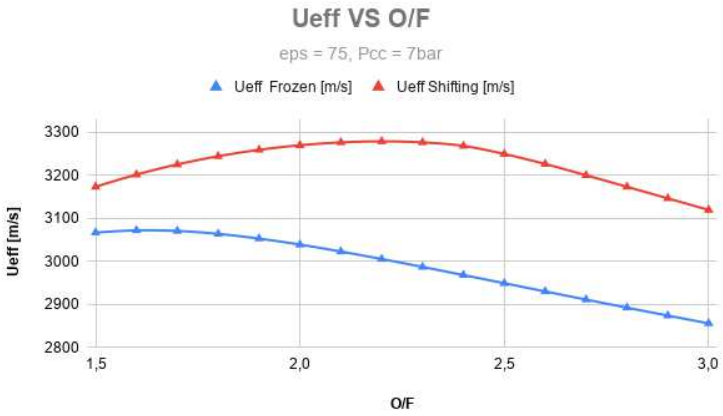

Figure 3: Effective velocity vs OF

After the decision of this parameter one can follow two approaches: the thrust approach (selecting the desired thrust and then sizing the whole propulsion unit) or the geometrical approach (selecting a geometrical parameter and then computing all the performances).
Since some geometry issues are present, a geometrical approach is followed. After having stated the CC radius at 10mm and the Mach number in the CC at 0.05 (this value is chosen because of the quite short dimensions of the unit), one can easily compute the throat area and the exit area. Consequently, the overall geometry of the engine is concluded by computing the CC length thanks to the L* parameter and its own volume.

Eventually, the CC wall thickness is evaluated considering the chamber as an ideal cylinder subjected to a radial load pressure. The minimum thickness is actually found. However due to manufacturing issues, it is increased up to 1mm. For the combustion chamber material, INCONEL 718 [16] is selected, due to its good response to mechanical and thermal loads.
INCONEL features the possibility of being 3D-printed, so complex and quite reduced geometries can be realized [21].

L_{CC}	5.93 cm
r_{CC}	1.00 cm
V_{CC}	18.62 cm^3
t	0.10 cm
L^*	70.00 cm
M_{CC}	0.05

Table 6: Combustion chamber characteristics

2.4 Conical Nozzle vs Rao's Bell Nozzle

At this stage the team has to design the nozzle accomplishing former goals and ensuring an acceptable level of losses. In this framework, two different nozzles are designed and compared.

The first approach considers a conical nozzle, knowing r_e and r_t from the previous process, the first design choice is to select the angle of the divergent part α. According to [13], typical values for α go from 12° to 18°. Given the geometric constraint, a value of 18° is chosen in order to reduce the length of the divergent part.

The same process has been undertaken to compute the angle of the convergent part, defined as β. For β, in accordance to the typical values, an angle of 45° seems to be reasonable for the reason previously explained. At this stage, all the parameters for the design are available and the computation gives the results shown in Tab. 7.

Associated to this configuration, λ factor is introduced in order to analyse the losses. It is calculated in the following way as suggested by [13]:

$$\lambda = \frac{1}{2}(1+\cos\alpha) \tag{1}$$

The second configuration considers the Rao approximation to size a bell-shaped nozzle. The choice of this design process is justified by the possibility to reduce even more the length of the divergent part of the nozzle. To design a Rao nozzle, a 60% length of the reference model's is thought to be reasonable to encounter the need of having a short thrust block. Of course, the lower the length, the higher the losses, that is why a control over the loss factor λ is performed also in this second design. To complete the configuration, the angles at inflection and exit point are taken from Rao's table. The two parameters α_{Rao} and λ_{Rao} are computed as follows:

$$\alpha_{\text{Rao}} = \arctan\left(\frac{r_e - r_t}{L_{\text{div}}^{\text{Rao}}}\right) \tag{2}$$

$$\lambda_{\text{Rao}} = \frac{1}{2}\left(1+\cos\left(\frac{\theta_e+\alpha_{\text{Rao}}}{2}\right)\right) \tag{3}$$

The results of the design are shown in Tab. 7:

α	18°
β	45°
L_{conv}	0.71 cm
L_{div}	6.86 cm
r_e	2.52 cm
r_t	0.29 cm
λ	0.9755

β	45°
θ_i	39.3°
θ_e	12.7°
L_{conv}	0.71 cm
L_{div}	4.99 cm
r_e	2.52 cm
r_t	0.29 cm
λ_{Rao}	0.9745

Table 7: Conical nozzle (on the left) and Rao nozzle (on the right)

The Rao nozzle (see Tab. 7) is able to provide both a quite short nozzle (divergent part) with respect to the conical one with $\alpha = 18°$ and a reasonable value of losses (looking at λ factor). For these motivations, the Rao Nozzle is implied in the motor design.
For the nozzle material, the same for the CC is selected. The idea is to manufacture a single piece in order to avoid connections with welding or bolts. To ease the process a constant 1mm thickness is considered.

2.5 Cooling system

Inside the thrust chamber an adiabatic flame temperature of about 3000 K is reached. Also for accomplishing the mission a total burning time of almost 40 sec is required.
The material of thrust chamber is INCONEL 718 [16], this one features a high mechanical resistance at high temperatures. However the working temperature is fixed to almost 1000K

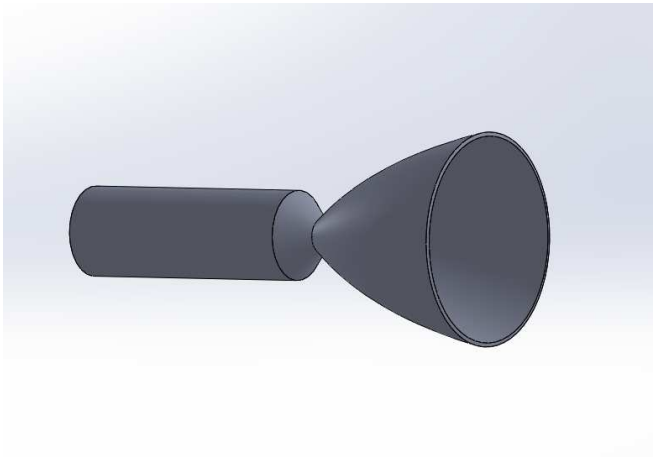

Figure 4: Engine Assembly

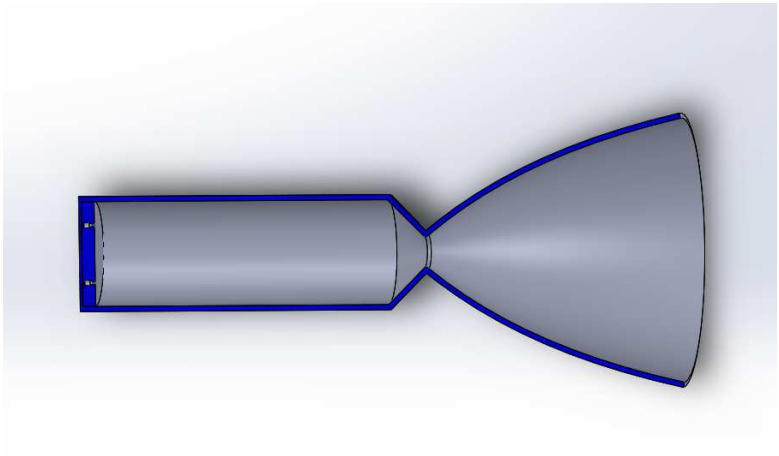

Figure 5: Engine Side Cut

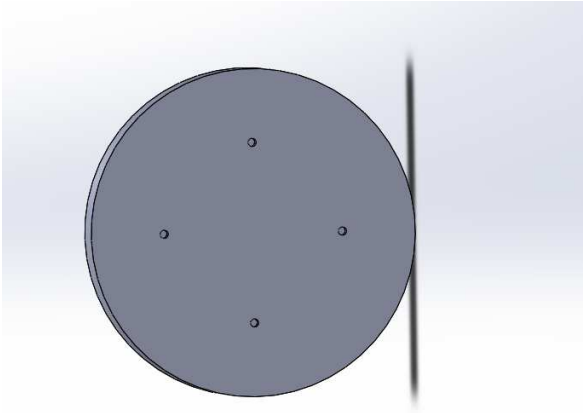

Figure 6: Injection Plate Particular

and the melting temperature is about 1500K.

So, in order to avoid a thermal failure in the material and consequently in the propulsive apparatus too, a cooling system is required. For this kind of application (low pressure chamber and pressure feed system), an ablative cooling system is recommended. For such of application, an ablative material of high-silica-cloth reinforcement and phenolic resin is employed [6].
In this system the fibres are oriented with an angle of 60 degrees with respect to the engine

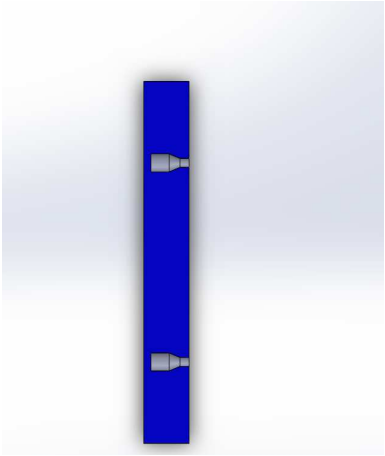

Figure 7: Injection Plate Side Cut

centreline. This ablative allows a quite reduced erosion in time, in addition with the quite short operating time a small amount of ablative is required. This small layer of ablative in accordance with its low rate of erosion allows a slight variation in the throat area.

2.6 Injectors

The rocket engine works with a very low pressure. This characteristic leads to consider the lowest possible value for the diameter of the orifices. Hence the configuration shown in Fig. 8 has been chosen.
From [13] the values reported in Tab. 8 have been selected.

D_h	0.5 mm
C_d	0.7

Table 8: Short tube with conical entrance [13].

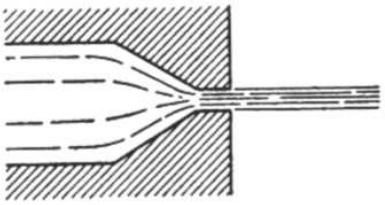

Figure 8: Short tube with conical entrance [13].

Furthermore, a configuration of 1OX-1F has been utilised.
Since the OX and F are both liquids, an impinging-stream-type is considered. Hence, the pressure drop is evaluated as the 20% of the chamber pressure.
These design choices have been selected since the mixing is accomplished in the combustion chamber by volatilization of the propellants and by turbulence. Indeed, they provide good inherent combustion stability at a moderate performance level. Applications have been successful for storable hypergolic propellant combinations [14].

The cross-sectional areas of the orifices can be designed once the pressure drop and the densities of the propellants are known:

$$A = \frac{\dot{m}}{C_d\sqrt{2\Delta P\rho}} \tag{4}$$

Equation (4) is used for both MMH and NTO.
By comparing the evaluated areas with the one of the single orifice, 2 orifices are obtained for the fuel; then the diameter of the orifices related to the oxidizer have been changed in order to obtain the same number. The sizes are reported in Tab. 9.
To evaluate the velocities when the oxidizer and the fuel impinge, the angle between the chamber axis and the average resultant stream is set as 0°, in order to achieve a good performance [13]. Also the angle of the oxidizer is fixed as 30°.

d_{OX}	0.5554 mm
d_F	0.5000 mm
γ_F	39.7753°

Table 9: Geometries related to the injectors.

2.7 Feed system

The feed system consists of the storage tanks for the propellant couple, the valves, the flow lines and the tank pressurization system.

Propellants tanks

The masses (reported in Tab. 10) of the NTO and MMH are evaluated through the product between the burning time and the respective mass flow rates. The values have been incremented of the 5% for safety reasons.
In order to evaluate the pressure in the tanks of the OX and F (see Tab. 10), the P_{CC} and the following losses (Tab. 10) have been summed [18] [13]:

$$\Delta P_{inj} = 20\% P_{CC} \tag{5}$$

$$\Delta P_{dyn} = \frac{1}{2}\rho u^2 \tag{6}$$

$$\Delta P_{feed} = \left(k_l + \lambda_l \frac{L}{D}\right)\frac{1}{2}\rho u^2 \tag{7}$$

for the ΔP_{feed}, see Paragraph **Feeding lines** in 2.7.

Since the maximum thrust requirement is low compared to the traditional satellite propulsion systems, a pressure-fed system is utilised [15].
Since the spherical tanks are the ones that minimise the mass for a given volume [13], this geometry has been chosen for the tanks.
Through the tensile strength [20]s [8] the thickness of the tanks have been computed as follows

$$t = \frac{P_b r_T}{2F_{TU}} \tag{8}$$

where the thickness of the tanks has been incremented of 0.5 mm for manufacturing feasibility.

Different materials (Al 2014-T6, Al 1100-O, Ti-6Al-4V), compatible with the couple, have been analysed and compared, in order to obtain a system with the minimum possible mass.

The selected material (Ti-6Al-4V) leads to the values reported in Tab. 10 and Tab. 11.

m_{OX}	0.2867 kg
m_F	0.1738 kg
P_{OX}	0.8413 MPa
P_F	0.8408 MPa

Table 10: Values related to OX and F (liquids) in the tanks.

$V_{T,OX}$	0.2021 dm^3
$V_{T,F}$	0.2037 dm^3
$m_{T,OX}$	26.3 g
$m_{T,F}$	26.4 g

Table 11: Values related to the tanks of OX and F.

Pressurised gas

In order to choose the pressurising gas two typical inert gasses have been compared: molecular nitrogen and helium.
Two different approaches have been carried out: firstly only a single pressurising gas tank and then two different ones have been examined. Since the first configuration exceeds the volume constraint, the latter has been utilised.
For each of them, the initial temperature has been fixed high enough to sustain a proper adiabatic expansion [18] (as reported in Tab. 12). Then the final temperature has been set slightly higher than the freezing one of the fuel and oxidizer respectively. The expansion stops once the pressure of the pressurising gas (i.e. the final one) is equal to the propellant one. Thus, by assuming an adiabatic expansion the initial pressure of the PG has been computed (see Tab. 12).

	Fuel	**Oxidizer**
$\mathbf{T_{in,PG}}$	340 K	340 K
$\mathbf{T_{fin,PG}}$	225 K	265 K
$\mathbf{P_{in,PG}}$	3.5662 MPa	2.0126 MPa
$\mathbf{P_{fin,PG}}$	0.8408 MPa	0.8413 MPa

Table 12: Temperatures and pressures related to the pressurising gas.

Firstly, by using the data in Tab. 12 and the Eq. (9) and (10), the final and initial volumes of the pressuring gas have been evaluated and also the mass through the ideal gas law.

For safety reasons [13], the found mass has been incremented of the 5% and then the volumes have been computed once again (through Eq. (11) and ideal gas law); the results are reported in Tab. 13.

$$V_{fin,PG} = \frac{V_T}{1 - \frac{P_{fin,PG}\, T_{in,PG}}{P_{in,PG}\, T_{fin,PG}}} \tag{9}$$

$$V_{in,PG} = V_{fin,PG} - V_T \tag{10}$$

$$V_{fin,PG} = V_{in,PG} + V_T \tag{11}$$

Since the nitrogen in this case is the inert gas that minimises the volume, it has been chosen as the pressurising one of the system.

	Fuel	Oxidizer
$V_{in,PG}$	0.1184 dm^3	0.2455 dm^3
$V_{T,PG}$	0.1270 dm^3	0.2582 dm^3
m_{PG}	4.2 g	4.9 g
$m_{T,PG}$	23.7 kg	35.1 g

Table 13: Masses and volumes related to the pressurising gas and their tanks.

Feeding lines and valves

For the feeding lines the selected material is Ti-3Al-2.5V [12] [7]. It offers 20 to 50% higher tensile strength than the commercially pure titanium and elevated temperatures.
It has excellent resistance to torsion and corrosion [12] and furthermore its roughness is 0.020 [19].

In order to obtain the dimensions reported in Tab. 14 the length and the diameter of the tubes have been fixed (see Tab. 14).
Then to guarantee the conservation of the mass flow, the velocities have been computed; thought Reynolds number and roughness, the Moody diagram has been exploited in order to get λ_l.
Moreover, the pressure losses have been evaluated as well as the geometric parameters reported in Tab. 14.

	OX tank → CC	F tank → CC	PG tank → OX tank	PG tank → F tank
L	0.1 m	0.1 m	0.165 m	0.165 m
D	3.25 mm	3.25 mm	3.25 mm	3.25 mm
t	0.504 mm	0.504 mm	0.504 mm	0.504 mm

Table 14: Dimensions related to the different feeding lines.

	On-off valve	Check valve	90° Angle Pipe (see Fig. 9)
k	0.1	2.7	0.24

Table 15: Values of the minor losses coefficient [9].

	OX tank → CC	F tank → CC	PG tank → OX tank	PG tank → F tank	Valve
m [g]	2.7	2.7	4.4	4.4	5

Table 16: Masses of the tubes and of each valve [10].

For each feed line two valves have been used: one check valve and one on-off; their coefficients of minor losses and their masses are reported respectively in Tab. 15 and Tab. 16.

3 Performance evaluations

3.1 Motor performances

Once the geometry of CC and nozzle are defined, one can easily evaluate the motor performances. Firstly the pressure ratio $\left(\frac{P_e}{P_{CC}}\right)$ is evaluated from the ϵ, then the outer pressure is found. Immediately after, the c* (engine characteristic velocity) is computed from the thermochemical properties of the combustion reaction [13].

This parameter alongside with the throat area and the P_{CC}, allows the evaluation of the propellant mass flow rate at the throat section. Consequently, from the pressure ratio and the expansion ratio, it is possible to directly compute the thrust coefficient [13].
From the definition of this parameter, one can estimate the thrust developed by the engine and the gravimetric specific impulse. Eventually, both the thrust and the specific impulse are corrected with the lambda factor for the nozzle divergence losses in the case of a Rao's nozzle.

$$T_{real}^{Rao} = \lambda_{Rao}\dot{m}_P u_e + A_e\left(P_e - P_{amb}\right) \tag{12}$$

Once all the engine-related performances are available, a preliminary evaluation for the propellant mass is carried out. This first iteration considers a fully occupied 6U-CubeSat. From the already-known initial mass, it is possible to evaluate the mass ratio from the Tsiolkovsky rocket equation, the final mass, the propellant mass and the burning time.

A more refined iteration is consequently performed, once a more accurate and refined estimation of the masses is available. From this value, in accordance with the previously computed I_{sp}, one is able to verify if the propulsion unit is capable of providing the required mission Δv.
If this statement is verified, one can tune the t_b (by fixing the propellant mass flow rate) to compute more precisely the effective required propellant mass.
At the end, the volumetric and total impulses are eventually evaluated.

	Ideal	Conical Nozzle	Rao Nozzle
F [N]	35.235	34.400	34.365
I_{sp} [s]	327.561	319.803	319.473
$I_{sp,V}[\frac{kg\,s}{m^3}]$	379145	370166	369784
$I_{sp,TOT}$ [Ns]	1409.388	1376.008	1374.588
t_b [s]	40	40	40

Table 17: Performance evaluation.

Accordingly to Rao nozzle, the new I_{sp} and the n_m, a new Δv is achieved as 623.40 $\frac{m}{s}$ (see Tsiolkovsky equation).

The obtained masses are:

	CC	Nozzle	PG_{TOT}	$Tanks_{TOT}$	$Tubes_{TOT}$	$Valves_{TOT}$	m_s
m [g]	32.0	55.9	9.1	111.5	14.2	40	500

Table 18: Inert masses.

	Inert	Initial	Final
m [kg]	0.7626	2.5531	2.0926

Table 19: Overall masses.

3.2 Centre of gravity

To evaluate the centre of gravity, the origin of the reference frame has been fixed in the geometric centre of the overall structure.
In particular, the c_G of each unit has been set in the geometric centres of themselves, but the unit related to the combustion chamber and the nozzle. Here, they firstly have been analysed as parts of a unique structure; since their geometry resulted too complicated to manage, it is not possible to consider their centre of gravity in the centre of the unit.
Thus, the latter coordinates have been evaluated through by using a CAD model.

Moreover, the masses of the feeding lines have been discarded since they are negligible.
The axes have been set as reported in Fig. 1. The position has been computed at the beginning and at the end of the mission, considering the propellant completely dumped.

$$c_G = \frac{\sum_{i=1}^{N} m_i c_{G,i}}{m_{TOT}} \tag{13}$$

where N and m_i are respectively the number of components of the structure and their masses, which are the four tanks, the nozzle, the combustion chamber and the payload.

	x [mm]	y [mm]	z [mm]
$c_{G,in}$	47.5	0	-7.7
$c_{G,fin}$	45.1	0	-1.0

Table 20: Centre of gravity coordinates.

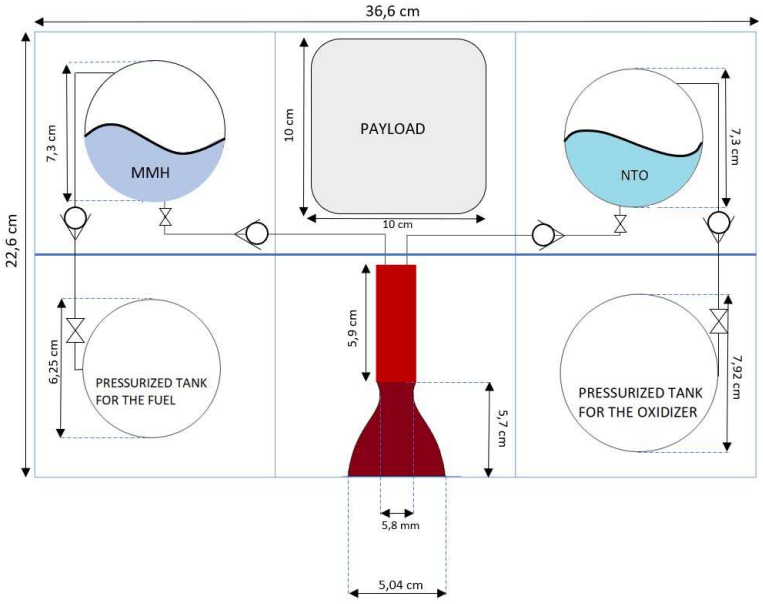

Figure 9: Scheme of the system

4 Possible failure modes

The structure is one of the simplest bi-propellant systems: it is a pressure-fed system with no pumps, shafts or moving parts. In addition, the reliability of the system has been the main focus of the project, in fact hypergolic propellants are chosen to avoid a catalyst bed or any ignition system devices. The major failure modes are:

- possible failures of valves, in particular the one-way valve. The rupture of this component could lead to the overall failure of the mission itself. Furthermore, a failure in one of the on-off valve at the beginning of the mission could affect the result of the whole mission.
- Possible leakages in the tanks and/or in the pipes feed lines. This mode could lead to a not-proper mass flow rate at the injection in the combustion chamber.
- In case of emergency, a sudden closing of the on-off valve could generate a water-hammer inside the pipes. The formation of this event could provoke a rupture in the pipes of the feeding-system.
- Formation of the boundary layer (BL) inside the nozzle. Since the throat radius is quite reduced (r_t = 2.9 mm), the BL effects are no more negligible. Therefore, the flow will experience a reducing in the throat area, so a concentration of thermal-fluid effects are present. This could possibly lead to a failure in the nozzle material and/or an off-design conditions.
- Not-properly glueing of the ablative layer at the CC and nozzle. A non-properly glueing could lead to the detachment of the ablative itself, provoking a physical choking of the nozzle, causing a critical failure in the entire propulsive system.

5 Concluding remarks

Given the geometric constraints in terms of volumes and space, the designed propulsion unit for the CubeSat generates a Δv equal to 623.40 $\frac{m}{s}$, capable of granting an orbit change manoeuvre.

Nowadays, in CubeSat applications monopropellants and their intrinsic simplicity are widely used and preferred with respect to bi-propellants. In fact, the latter introduce a higher degree of plants' complexity due to their needs of a pressurizing and injection systems. However, this analysis shows that such an application, based on MMH and NTO, can grant good performances in terms of Δv limiting at the same time structural weights and volumes.
Therefore, the analysis of the bipropellant propulsion devices can be useful to have a wider application of this challenging technology, providing a primary propulsion source.
From the performed computations it results that the centre of gravity is not aligned with the thrust chamber, neither at the beginning nor at the end of the mission. Consequently, a dynamic controller for thrust direction or a gimbaled thrust system could be adopted. Using the latter, the engine or just the exhaust nozzle of the rocket can be swivelled on two axes (pitch and yaw) from side to side. As the nozzle is moved, the direction of the thrust is changed relatively to the centre of gravity of the rocket [3]. Since the gimbaled thrust system is not yet available in a miniaturized version, this is left for future researches.
Moreover, a membrane in EPDM could have been chosen, in order to avoid the collision between the pressurizing gas and the propellant. Indeed, EPDM is an extremely durable synthetic rubber membrane; its two primary ingredients, ethylene and propylene, are derived from oil and natural gas [4].

Nowadays, the requested dimensions for the membrane are not exploited; however, this could be a subject for future developments.
Indeed, with the development of complex bi-propellants systems in small volumes, the horizons of manufacturing can be enlarged by introducing new technologies and materials. These improvements would allow the implementation of more efficient components that increase the performance of the systems and could give wider applications for CubeSats.

References

[1] Aerojet rocketdyne in space propulsion datasheet.

[2] Design and analysis of combustion chamber and nozzle of rocket engine by using inconel 718.

[3] *(NASA) Gimbaled Thrus. Beginner's Guide to Rockets*. Public domain source, Retrieved 2006-01-07.

[4] M. Aerospace. Spacecraft propellant tanks.

[5] W. S. U. K. . U. Akshay Reddy Tummala, Atri Dutta (Department of Aerospace Engineering. *An Overview of Cube-Satellite Propulsion Technologies and Trends*. 9 December 2017.

[6] J. N. Arthur M. Shinn. *Experimental evaluation of six ablative-material thrust chambers as components of storable-propellant rocket engines*. Lewis Research Center, Cleveland, Ohio, June 1967.

[7] S. M. Centres. Ti-3al-2.5v (grade 9) titanium alloy.

[8] S. M. Centres. Ti-6al-4v (grade 5) titanium alloy.

[9] L. Danizzi. *Le perdite di carico nei circuiti idraulici*. ECOACQUE.

[10] I. Donald Platt (Micro Aerospace Solutions. *A Propulsion System Tailored to Cubesat Applications*. 21st Annual AIAA/USU Conference on Small Satellites.

[11] Endurosat. 6u cubesat platform.

[12] finetubes. Titanium alloy ti 3al/2.5v.

[13] O. B. George P. Sutton. *Rocket Propulsion elements*. Wiley - 9th edition, 2017.

[14] Huzel and H. (NASA). *Design of liquid propellant rocket engines*. Second edition.

[15] F. T. P. d. M. I. A. C. D. U. o. T. t. N. Karthik Venkatesh Mani (Politecnico di Milano, Italy). *Chemical Propulsion System Design for a 16U Interplanetary CubeSat*. 69th International Astronautical Congress, Bremen, Germany.

[16] U. P. Metals. Nickel alloy inconel 718 - properties and applications.

[17] T. Program. *6U CubeSat Platform*. CP-6UCDS-1.0.

[18] W. B. Ronald W. Humble. *Humble space propulsion analysis and design*. McGraw-Hill Companies, 1995.

[19] R. Vasilev. *Study of the Mechanical Properties of Ti-3Al2.5V after Surface Plasma Gas Treatment with Indirect Plasma Torch*. TEM Journal, Technical University.

[20] B. S. Wanhill, Russell. *Metallurgy and Microstructure, Fatigue of Beta Processed and Beta Heat-treated Titanium Alloys*. Springer Netherlands, 2012.

[21] A. Young. *The Saturn V Booster: Powering Apollo into History*. Springer-Verlag, 2009.